

Mid-infrared imaging of AGB star envelopes

II. Modelling of observed sources

M. Marengo¹, G. Canil², G. Silvestro², L. Origlia³, M. Busso³, and P. Persi⁴

¹ International School for Advanced Studies, Trieste, Italy

² Dipartimento di Fisica Generale, Università di Torino, Italy

³ Osservatorio Astronomico di Torino, Pino Torinese, Italy

⁴ Istituto di Astrofisica Spaziale, CNR, C.P. 67, I-00044 Frascati, Italy

Received 23 July 1996 / Accepted 10 December 1996

Abstract. Radiative transfer modelling of AGB circumstellar envelopes is applied to a sample of AGB stars previously observed with the mid-IR imaging camera TIRCAM (Busso et al. 1996: Paper I). We present the results of our simulations, aimed at deriving the physical parameters of the envelope, such as its optical depth, radial thermal structure, mass loss and dust-to-gas mass ratio. The chemical composition of the dust in the observed envelopes is discussed. The ability of different sets of dust opacities to fit the mid-infrared spectra is evaluated. The hypothesis of dust grain aging and annealing in O-rich envelopes is considered in order to explain an apparent inadequacy of the available opacities to describe the variety of observed spectra, as previously noted by other authors. Various possible origins of the discrepancies are discussed, together with their consequences on the dust grain formation processes.

Key words: infrared: stars – stars: circumstellar matter – stars: AGB – radiative transfer

1. Introduction

Asymptotic Giant Branch (AGB) stars are characterized by intense mass loss processes that play a central role in the star's subsequent evolution and lead to the formation of a cold circumstellar envelope (CSE) of gas and dust. The envelope chemical composition is determined by the amount of carbon enrichment in the stellar atmosphere, due to mixing processes (the so called *third dredge-up*), induced by thermal pulses near the end of the AGB phase. C-rich envelopes (having $[C]/[O] > 1$ by number) mainly exist around carbon stars, while O-rich CSEs ($[C]/[O] < 1$) are associated to M giants. The transition from O-rich to C-rich envelopes is controlled by the extent of the third dredge-up, and it can occur only for AGB stars in a

narrow mass range: indeed, stars with a core mass lower than $0.6 M_{\odot}$ (Straniero et al. 1995) are unable to undergo the third dredge-up, while H burning at the base of the convective envelope (Hot Bottom Burning) is expected to deplete carbon in the envelope of stars more massive than $\sim 5 M_{\odot}$ (Wood et al. 1983; Boothroyd et al. 1993; Frost & Lattanzio 1995), preventing them from becoming C-rich.

Despite the low dust-to-gas mass ratio (in the range ~ 0.001 – 0.01), the optical properties of AGB CSEs are mainly determined by the dust grains: silicates in O-rich envelopes (Pégourié & Papoular 1985) and a mixture of Hydrogenated Amorphous Carbon (HAC, Jones et al. 1990; Duley 1993) with inclusions of SiC (Skinner & Whitmore 1988) and possibly Polycyclic Aromatic Hydrocarbons (PAH, Puget & Léger, 1989; Cherchneff & Barker 1992) in C-rich CSEs. Both oxidic and carbonaceous star dust is characterized by vibrational bands positioned in the mid-IR window (at 9.7 and 18 μm for silicates, at 11.3 μm for SiC and at 3.3, 6.2, 7.7, 8.6 and 11.3 μm for PAH); furthermore, most of the continuous thermal radiation from the dusty optically opaque envelope is emitted in the same wavelength range.

For these reasons a mid-IR search was carried out with the imaging camera TIRCAM (Busso et al. 1996, hereafter Paper I) for a sample of 16 sources, including both AGB (O-rich and C-rich) and post-AGB stars. In Paper I, photometry and colors were derived using 10% bandwidth filters at 8.8, 9.8, 11.7 and 12.5 μm , and compared with the Low Resolution Spectra (LRS) from IRAS (1986), in order to establish suitable photometric criteria for discriminating between O-rich and C-rich sources and for estimating mass loss rates. The observations formed the basis for discussing the evolutionary status of the sources and their mass loss history. In Sect. 2 we discuss the general features of their spectra, from the point of view of the optical properties that can be inferred for dust.

Detailed numerical simulations of the CSE thermal structure is the subsequent step for a better determination of the physical parameters. One has to compute the source spectrum and

the radial brightness distribution for a wide range of input parameters; comparison with observations will then allow us to estimate the optical depth of the envelopes, to derive mass loss rates, and to extract information on chemical abundances which are relevant to study the stellar nucleosynthesis (see e.g. Busso et al. 1995). With these aims in mind, we developed a numerical code for solving the problem of non-grey radiative transfer through a spherically symmetric dust shell around an evolved AGB star. We present our model in Sect. 3, with emphasis on the input model parameters and on the dust opacities used. In Sect. 4 the model results are shown for the sources observed in Paper I whose LRS is known, and a new estimate for the dust mass loss rates and the dust-to-gas mass ratio is obtained.

In Sect. 5 a more general discussion of the model spectra is carried on. We point out how available dirty silicates dust opacities alone seem not to be completely adequate for a detailed simulation of the mid-IR features of circumstellar dust, as previously suggested by different authors (Onaka et al. 1989ab; Little-Marengin & Little 1990, hereafter LML90; Simpson 1991), and we test possible explanations. Our conclusions are summarized in Sect. 6.

2. Spectra of AGB circumstellar envelopes

The IRAS color-color diagram (van der Veen & Habing 1988) obtained by IR photometry at 12, 25 and 60 μm , provides a first-order discrimination of AGB sources, according to their infrared excess, variability and C abundance. However, as shown in Paper I, such IRAS color-color diagram can lead to misclassification of AGB CSEs due to the large width of IRAS filters (this is true in particular for the one at 12 μm , which cannot discriminate between silicates and carbonaceous features). Although narrow band filters allow a better discrimination (as in the case of TIRCAM photometric system), a detailed description of the dust emission/absorption features requires mid-IR spectra.

IRAS LRS (1986) provide spectral energy distributions in the wavelength range 7.7–22.6 μm for about 4,000 AGB sources, which are classified with a two-digit code. The first digit (main class) is related to the spectral index β of the continuum (assuming $F_\lambda \propto \lambda^\beta$), while the second indicates the strength of the main feature, in emission or absorption, present in the mid-IR window. In particular, spectra of O-rich sources are identified by the 9.7 μm silicate feature, that is found in emission or absorption in the LRS classes $2n$ and $3n$, respectively. C-rich envelopes are mainly found in the $4n$ class, defined by the presence of the 11.3 μm SiC feature in emission. Post-AGB objects of both types are in the main classes $6n$ and $7n$, characterized by very large infrared excess. Finally, both O-rich and C-rich sources may fall in classes $1n$ and $0n$ (featureless spectra), where a few LRS with self-absorbed SiC feature can be found (Omont et al. 1993).

Table 1 lists the spectral characteristics of the sources in Paper I with known LRS; the star AFGL 1822 was added to the TIRCAM sample in order to have an evolved O-rich envelope with the 9.7 μm silicate feature in absorption. Post-AGB sources

Table 1. List of AGB sources from Paper I with known LRS. The evolved O-rich envelope AFGL 1822 was added to have a $3n$ LRS class source. Last column: LML90 LRS subclass, when available.

#	IRAS name	Name	Type	SP type	LRS	LRS sub.
1	02143+4404	W And	S-star	S8,2e(M)	22	S
2	08525+1725	X CnC	C-rich	C5,4(SRb)	42	—
3	09425+3444	R LMi	O-rich	M7e(M)	24	Sil+
4	09452+1330	CW Leo	C-rich	Ce(M)	43	—
5	12427+4542	Y CVn	C-rich	C5,5J(SRb)	42	—
6	13001+0527	RT Vir	O-rich	M8III(SRb)	21	—
7	15193+3132	S CrB	O-rich	M6,5e(M)	24	Sil+
8	15255+1944	WX Ser	O-rich	M8e(M)	29	Sil
9	16029-3041	AFGL 1822	O-rich	M	32	—
10	16235+1900	U Her	O-rich	M7IIIe(M)	23	Sil+
11	18040-0941	FX Ser	C-rich	C(Lb)	44	—
12	18397+1738	NSV 11225	C-rich	Ce	43	—

have not been included because their modelling involves very different physical conditions, dominated by the hot radiation emitted by the central star (B or A spectral type) on its way to become a white dwarf.

Note that the LRS class $2n$ contains sources with different characteristics; a tentative classification is in the LML90 paper, where the silicate band profiles in optically thin O-rich envelopes are divided into seven subclasses, according to their shape and the presence of secondary peaks. The subclass for our O-rich sources, when given by LML90, is reported in Table 1; the S-star W And is tentatively attributed to the “S” feature subclass, characterized by a broad peak at 10.3 μm . The other sources fall in subclass “Sil” (with a strong feature peaked at 9.8 μm , typical of $2n$ LRS with $n > 4$) and subclass “Sil+” (having a secondary “bump” at 11.3 μm). LML90, and Simpson (1991) suggest that these differences be related to a kind of “mineralogical diversity” in the oxidic CSE dust, although this explanation is still controversial (see e.g. Ivezić & Elitzur 1995, hereafter IE95). We tried to model the shape of the silicate feature in our sources belonging to different subclasses using several sets of opacities and dust mixtures.

3. Our model

Radiative transfer in circumstellar dust shells has been previously discussed by many authors (Rowan-Robinson 1980; Griffin 1990; Justtanont & Tielens 1992, Groenewegen, 1993 and, more recently, Hashimoto 1995; a detailed discussion of these models is given in Habing, 1996). A fully self-consistent modelling of envelopes around evolved late-type stars requires coupling of radiative transfer with the time-dependent hydrodynamic equations of motion for the two interacting fluids (gas and dust) which constitute the stellar wind. Such an approach has been attempted by IE95: their treatment, in the hypothesis of a steady-state outflow due to constant dust-driven stellar wind, can successfully account for the observed mass loss rates and is able to reproduce the IRAS colors and visibility functions (see Ivezić and Elitzur 1996a, b) for a large sample of AGB objects in all LRS classes. More recently, models taking into account time

dependent hydrodynamics have been developed to study the effect of sudden variations in the stellar parameters in connection with thermal pulses (Schönberner et al. 1996). This analysis is necessary in order to follow the latest stages of AGB evolution, which lead to the formation of a planetary nebula; however, time variations of the mass loss rate, on a thermal pulse time scale, have negligible effects on the IR properties of at least 95% of late-type stars associated with IRAS sources (IE95).

Further, two fluid (dust and gas) models for stationary dust-driven winds treating dust formation (with classical nucleation theory) and equilibrium chemical reactions have been developed to determine the gas molecular composition, dust to gas mass ratio and total mass loss in a self consistent way (Krüger et al. 1994)

In our model we totally neglect the dynamics of the envelope and the details of dust formation (the mass loss rate is a free parameter that is determined by fitting the data); rather, we concentrate our efforts on obtaining an accurate fit of the observed sources, paying special attention to the mid-IR interval, where the TIRCAM spectral bands are located (see Paper I). The model parameters are fixed by fitting the IRAS and TIRCAM data. For any dust mixture, the spectrum (and in particular the shape of the features) is used to estimate the optical depth τ_ν of the envelope, proportional to the dust opacity and the mass loss rate. Near- and Mid-IR photometric data allow us to determine the stellar parameters T_{eff} , R_* (the central star is assumed to radiate a black body spectrum at temperature T_{eff}), and the inner CSE radius R_1 ; the outer radius R_2 is derived by fitting the IRAS far-IR photometry at 60 and 100 μm . The source distance enters in the model only as a scale factor for the flux densities, and is determined by normalizing the spectra with the observed photometry. We first assumed the value estimated by Loup et al. (1993); then we computed our own value of $d = \sqrt{L_*/F_{1kpc}}$, where $L_* = 4\pi\sigma R_*^2 T_{eff}^4$ is the total luminosity and F_{1kpc} the total flux (in L_\odot , assuming a reference distance of 1 kpc) obtained by Loup et al. (1993) using IRAS fluxes.

The code computes iteratively a self-consistent thermal structure of the envelope; the emergent spectra is calculated taking into account the effect of non-isotropic scattering, absorption and thermal reemission by grains. The computation is performed on the hypotheses of: (i) spherical symmetry of the dust shell, with an $n(r) \propto r^{-2}$ density distribution, consistent with a steady outflow at constant velocity, (ii) balance between absorption and emission by the dust grains, and (iii) LTE dust radiation at the local temperature $T(r)$.

The dust grain composition is simulated adopting different sets of dust opacities Q_ν ; the dust grain size is usually assumed to satisfy a size distribution $n(a) \propto a^{-3.5}$ with $0.01 \mu\text{m} \lesssim a \lesssim 0.25 \mu\text{m}$ (Mathis, Rumpl and Nordsieck 1977, hereafter MRN; see e.g. Jura, 1996 for more recent data). The main effect of considering a grain size distribution is a broadening of the 9.8 μm silicate feature (Simpson 1991), due to the non linear dependance of the opacity on a ; this is however important only for $\lambda \lesssim a$ and in the case of AGB CSE grains can be neglected. Hence we simply adopted for the grain size the average MRN value $a = 0.1 \mu\text{m}$.

3.1. Dust opacities

Following a Chan & Kwok (1990) scaling theorem, the solution of the radiative transfer equation in spherical symmetry is scaled on the flux-averaged optical depth $\tau_F = \int_0^\infty \tau_\nu F_\nu d\nu / \int_0^\infty F_\nu d\nu$, where:

$$\tau_\nu = \pi a^2 Q_\nu \int_{R_1}^\infty n(r) dr \quad (1)$$

In Eq. 1, τ_ν depends on frequency only through the opacity Q_ν , which is thus the main parameter for modelling the spectra; for this reason, a great part of our preliminary work consisted in testing the various opacity profiles available in the literature. We now present the results of our analysis, separately for O-rich and C-rich dust.

It is well known that O-rich dust contains essentially silicate grains: they can be present as piroxens (Mg,Fe)SiO₃, or as olivinae ((Mg,Fe)₂SiO₄). Actually, the olivina opacity profile of Krätschmer & Huffmann (1979) is suitable for supergiants, but not for Miras like WX Serpentis (see Griffin 1993). In the case of circumstellar envelopes the silicate dust probably consist of piroxens only, with various types of impurities making them “dirty silicates”. We considered five opacity profiles for astronomical silicates.

The first is the one by Jones & Merrill (1976); they introduced the concept of “dirty silicates”, though many details of their opacity profile were subsequently modified.

The second is by Draine & Lee (1984); despite its wide use and accuracy, this is not well suited for our needs, since it is based on observations of the interstellar medium, and not of the circumstellar one (see also Ossenkopf et al. 1992, hereafter OS92, and Griffin 1993).

The third is by Volk & Kwok (1988); it is based on the observed spectra of 467 AGB stars with good quality photometric data in all four IRAS bands; the spectrum obtained from this opacity is similar to the observed one, but the 9.8 μm feature is slightly too much asymmetric and its peak is shifted towards redder wavelengths.

The fourth profile is the one by OS92: it is based on the previous but it is chemically and physically consistent, in the sense that computes the complex dielectric function for the dust using the Kramers-Krönig relations along with the Mie theory. Taking into account the possibility of dust annealing in the CSE, as illustrated by Stencel et al. (1990) and Nuth and Hecht (1990), the authors give the opacity in two versions, one for “warm” silicates (hereafter Oss1) and the other for “cold” ones (hereafter Oss2), depending on the physical conditions at their condensation.

The last and more recent is by David & Pégourié (1995), and is computed using Mie theory for a set of more than 300 IRAS sources with known LRS.

We obtained the best results when fitting our AGB O-rich sources with OS92 Oss1 and Oss2 opacities.

In the case of C-rich envelopes, the continuum in the spectra is usually ascribed to the presence of graphite or amorphous

carbon, while the characteristic band at $11.3 \mu\text{m}$ is commonly attributed to SiC, although the presence of PAH has been proposed as well. Graphite is now commonly ruled out, because of the absence in the observed spectra of its typical narrow band at $11.52 \mu\text{m}$ (Draine 1984); moreover, the whole shape of the spectra obtained by using graphite (the most used opacities are by Draine & Lee 1984) does not fit the observed ones, as we tested directly. Therefore the main constituent of CSE carbonaceous dust seems to be amorphous carbon: due to the variability in its physical and optical properties, a comparison with observational data is fundamental. An accurate enough opacity profile, observationally tested for amorphous carbon is the one by Martin & Rogers (1987). More recently Rouleau & Martin (1991) presented a detailed study giving accurate sets of optical constants derived by Bussoletti et al. (1987): the set named AC1, in particular, is similar to the Martin & Rogers (1987) opacity, although more detailed; this is the opacity we used for our simulations.

Finally, in order to obtain spectra with the characteristic $11.3 \mu\text{m}$ band, we admitted the presence of SiC mixed with the amorphous carbon: we choose the opacity set for α -SiC (the exagonal rhomboedric crystalline form of SiC) from Pégourié (1988), which at the moment is the only accurate profile available in the literature; to obtain the optical properties for the mixture, we simply made a weighted average of the two species: we never found necessary to take a SiC percentage greater than 10%. This strongly depends on the opacity chosen for amorphous carbon; IE95, for example, used a more absorptive kind of amorphous carbon, together with Pégourié (1988) data for SiC, and found a SiC percentage up to 30%.

In Fig. 1 we plot the final opacity profiles for silicates, amorphous carbon and SiC used in our simulations.

In our simulations we have not introduced Polycyclic Aromatic Hydrocarbons (PAH), because they are mainly excited by UV radiation, and their contribution to the dust heating and the final spectra is low for AGB stars, at least if a hot star companion is not present (Buss et al. 1991).

4. Model results

In order to fit the IR spectra of the sources in our sample, for each set of dust opacities we computed a grid of models parameterized on the $10 \mu\text{m}$ optical depth τ_{10} , which is proportional to the dust mass loss rate of the envelope:

$$\dot{M}_d = \frac{16\pi}{3} \frac{\rho_d a}{Q_{10}} \tau_{10} R_1 v_e \quad (2)$$

where ρ_d is the density of the dust grains (we assumed 3.0 g/cm^3 for OS92 silicates, 1.85 g/cm^3 for AC1 amorphous carbon and 2.5 g/cm^3 for Pégourié 1988 SiC), Q_{10} is the opacity at $10 \mu\text{m}$, and v_e is the outflow velocity of the dust. The models were computed assuming $d = 1 \text{ kpc}$, $R_* = 10^{13} \text{ cm}$, $T_* = 2500 \text{ K}$, $R_2 = 2000 R_1$, $R_1 = 4 R_*$ if $\tau_{10} < 1$ and $R_1 = 5 R_*$ if $\tau_{10} > 1$.

Fig. 2 shows model spectra (in the wavelength interval $1\text{--}100 \mu\text{m}$) of O-rich envelopes for increasing $\log \tau_{10}$, from -3 to

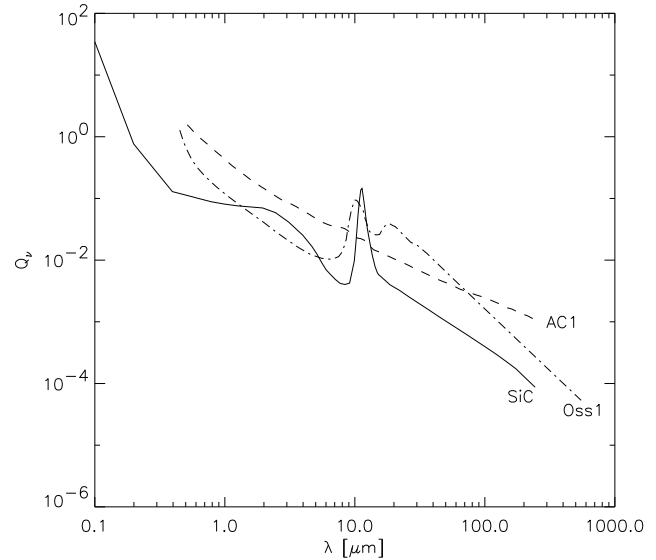


Fig. 1. Dust opacities used in our computations: Ossenkopf 1 “dirty silicates” profile by OS92 (dot-dash-dot line), amorphous carbon AC1 by Rouleau & Martin 1991 (dashed line) and Pégourié (1988) SiC (dotted line).

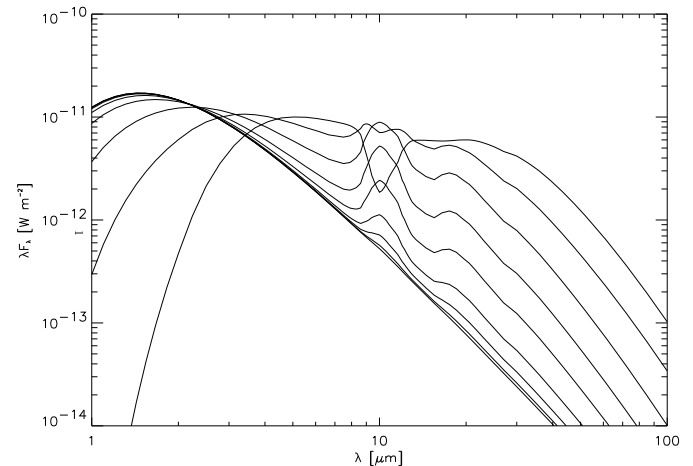


Fig. 2. Model spectra for O-rich circumstellar envelopes; the curves have $\tau_{10} = 0.001, 0.003, 0.01, 0.03, 0.1, 0.3, 1.0, 3.0$ and 10.0 ; the IR excess increases with increasing optical depth.

1; in Fig. 3 the sequence of C-rich models with $\log \tau_{10}$ from -3 to 0 is plotted. In both cases greater optical depths cause larger infrared excesses, and the dust features (silicates $9.8 \mu\text{m}$ and SiC $11.3 \mu\text{m}$) change from emission to absorption. We stopped the C-rich sequence at $\tau_{10} = 3$ because this can be taken as a limit for this class of sources, considering that SiC features in absorption are rare in the LRS database (see Omont et al. 1993).

The van der Venn & Habing (1988) IRAS color-color diagram for the computed model sequences is shown in Fig. 4. The two curves are associated to increasing optical depth, and thus to increasing mass loss; note that they cross the appropriate regions of the diagram for the two classes of sources. The curves should not be considered as evolutionary tracks, because there

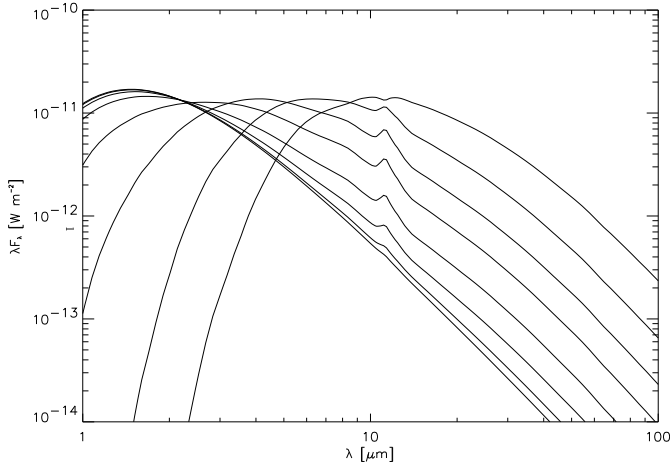


Fig. 3. Same as Fig. 2, for C-rich circumstellar envelopes having $\tau_{10} = 0.001, 0.003, 0.01, 0.03, 0.1, 0.3, 1.0$ and 3.0 .

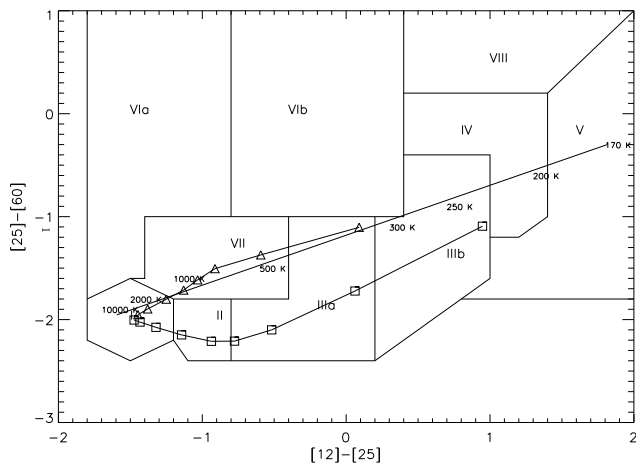


Fig. 4. IRAS [25]-[60] vs. [12]-[25] color-color diagram for O-rich (squares) and C-rich (triangles) model in Fig. 2 and 4 respectively; increasing optical depth results in increasing IR excess (from left to right).

is indication that mass loss rates do not increase monotonically during AGB evolution, rather they can have sudden variations in connection with thermal pulses (Vassiliadis & Wood 1993; see also Paper I).

4.1. Spectral distribution

By means of our model we finally fitted the spectral distribution of the sources listed in Table 1 and we obtained some relevant physical parameters for the star (T_{eff} , R_*) and the envelope (R_1 , R_2 , τ_{10}).

Moreover, we derived the dust mass loss \dot{M}_d (using Eq. 1, with v_e from Loup et al. 1993) and the bolometric luminosity $L_{tot} = 4\pi\sigma R_*^2 T_{eff}^4$.

From Loup et al. (1993) we also obtained values (based on radio OH and HCN observations and IRAS data) for the total mass loss rate \dot{M} and the total emitted fluxes $F_{1kpc} =$

Table 2. Model estimates for sources in Table 1. Envelope optical depth τ_{10} , dust mass-loss \dot{M}_d , dust to gas ratio μ , total luminosity L_* and distance d for each source are determined by model fitting parameters, while total mass loss \dot{M} , total fluxes F_{1kpc} and gas outflow velocities v_e are derived by IR-radio-millimetric observations from Loup et al. 1993.

#	Name	τ_{10}	v_e km/s	\dot{M} M_\odot/yr	\dot{M}_d M_\odot/yr	μ %	L_* L_\odot	F_{1kpc} L_\odot	d kpc
1	W And	0.17	20.	$9.7 \cdot 10^{-7}$	$2.5 \cdot 10^{-9}$	0.26	$2.9 \cdot 10^4$	$4.4 \cdot 10^4$	0.26
2	X ChC	0.15	9.7	$4.6 \cdot 10^{-7}$	$1.5 \cdot 10^{-9}$	0.33	$1.3 \cdot 10^4$	$2.1 \cdot 10^4$	0.79
3	R LMi	0.15	7.0	$5.0 \cdot 10^{-7}$	$1.0 \cdot 10^{-9}$	0.20	$5.7 \cdot 10^3$	$9.4 \cdot 10^4$	0.25
4	CW Leo	1.30	15.	$4.8 \cdot 10^{-5}$	$5.0 \cdot 10^{-8}$	0.10	$4.6 \cdot 10^4$	$6.6 \cdot 10^5$	0.26
5	Y CVn	0.01	8.2	$2.8 \cdot 10^{-7}$	$1.7 \cdot 10^{-10}$	0.06	$6.0 \cdot 10^3$	$8.7 \cdot 10^4$	0.26
6	RT Vir	0.15	9.3	$1.3 \cdot 10^{-6}$	$4.3 \cdot 10^{-9}$	0.33	$5.9 \cdot 10^4$	$1.3 \cdot 10^5$	0.67
7	S CrB	0.15	6.3	$6.0 \cdot 10^{-7}$	$8.0 \cdot 10^{-10}$	0.14	$4.6 \cdot 10^3$	$2.3 \cdot 10^4$	0.45
8	WX Ser	1.30	8.8	$5.3 \cdot 10^{-7}$	$8.2 \cdot 10^{-9}$	1.55	$3.2 \cdot 10^3$	$7.2 \cdot 10^3$	0.67
9	AFGL 1822	8.00	17.	$2.5 \cdot 10^{-5}$	$2.0 \cdot 10^{-8}$	0.08	$1.2 \cdot 10^4$	$2.8 \cdot 10^3$	2.10
10	U Her	0.15	13.	$2.6 \cdot 10^{-7}$	$1.1 \cdot 10^{-9}$	0.42	$1.1 \cdot 10^3$	$3.2 \cdot 10^5$	0.06
11	FX Ser	0.20	26.	$1.2 \cdot 10^{-5}$	$1.7 \cdot 10^{-8}$	0.14	$8.1 \cdot 10^3$	$8.4 \cdot 10^3$	0.98
12	NSV 11225	0.02	14.	$9.1 \cdot 10^{-6}$	$1.1 \cdot 10^{-8}$	0.12	$1.2 \cdot 10^4$	$2.8 \cdot 10^4$	0.65

$4\pi(1 \text{ kpc})^2 F_{total}$; we thus estimated the dust to gas ratio μ (in mass fraction) and the distance d for each source. Our results are summarized in Table 2.

Note that the dust to gas ratios are generally low ($\sim 10^{-3}$), with the exception of WX Ser. We would like however to stress that estimates of μ are affected by uncertainties in the grain average radius a ; Eq. 2 shows that \dot{M}_d is proportional to a (assuming a correct fitting of τ_{10}), which is not, in this case, simply a normalization factor. The distances we obtained are all in agreement with estimates by other authors (see e.g. Loup et al. 1993), with the exception of U Her, whose distance is clearly underestimated by our model, as explained below.

Fig. 5 shows the model spectra for a few sources reported in Table 1, superimposed to the IRAS LRS. All sources except those O-rich with less prominent silicate features (LML90's ‘‘Sil+’’, as in the case of U Her and ‘‘S’’ subclasses) can be satisfactorily fitted by the available opacities. In the case of the S-star W And (‘‘S’’ subclass), to fit the LRS spectra was necessary to use a mixture of silicate and carbonaceous dust in the proportion 1:4, being impossible to model the source using silicates dust only. The models for the sources with weak silicate features in subclass ‘‘Sil+’’ were obtained by fitting the continuum only; this allows us to produce reasonable values for the physical parameters listed in Table 2, but is not able to reproduce the correct profile of the dust feature. In our opinion, this is probably related to an inadequateness of the available silicate dust opacities for sources of LRS subclass ‘‘Sil+’’ and ‘‘S’’, but we discuss other possibilities in Sect. 5.

4.2. Temperature profiles

In spherical symmetry, the thermal structure of the model is expressed by a radial law $T(r)$ giving the self-consistent dust radiative equilibrium temperature for the dust grains. The temperature profiles thus obtained depend on the dust chemical composition and on the optical depth. For large envelope radii they can be approximated by a power law $T(r) \propto r^{-\alpha}$, where

Table 3. Asymptotic values of the thermal structure power-law exponent for the modelled sources, ordered for chemical type and increasing optical depth τ_{10} .

Name	τ_{10}	α
O-rich sources		
R LMi	0.15	0.348
RT Vir	0.15	0.349
S CrB	0.15	0.344
U Her	0.15	0.349
WX Ser	1.30	0.347
AFGL 1822	8.00	0.332
S source		
W And	0.17	0.385
C-rich sources		
Y CVn	0.01	0.397
Y CVn	0.01	0.397
X CnC	0.15	0.400
FX Ser	0.20	0.404
NSV 11225	0.20	0.404
CW Leo	1.30	0.404

α is the asymptotic value for the logarithmic derivative of the temperature profile $T(r)$:

$$\alpha = \lim_{r \rightarrow \infty} - \frac{d \log T}{d \log r} \quad (3)$$

The inferred α values are restricted to a limited range (see Table 3); however those for O-rich sources are systematically lower than those for C-rich ones (0.35 vs 0.40), while the case of the S-star modelled with a mixed dust composition is intermediate. This numerical result is in good agreement with the analytic formula first derived by Sopka et al. (1988) for spherically symmetric dust shells having power-law opacity $Q_\nu \propto \lambda^{-\beta}$ and density $n(r) \propto r^{-2}$:

$$T(r) \propto r^{-2/(4+\beta)} \quad (4)$$

For Oss1 silicates $\beta \simeq 2$ in the mid- and far-IR wavelength range, while for AC1 Rouleau and Martin amorphous carbon is $\beta \simeq 1$ in the same spectral range; Eq. 4 would give $\alpha \simeq 0.33$ for silicates and $\alpha \simeq 0.40$ for amorphous carbon, similar to our results, appropriate for the outer parts of the envelopes, where the mid- and far-IR thermal radiation is emitted.

5. Discussion

In order to account for the difficulties we found in modelling the O-rich envelopes of subclass “S” and “Sil+”, several possibilities can be considered: deviation from spherical symmetry,

mixing between O-rich and C-rich dust and necessity of new opacities for silicates producing LRS other than “Sil” subclass.

Evidences for non-spherical symmetry of AGB CSEs arise from radio mapping, speckle interferometry, polarization studies and spectroscopic observations as well as from the shapes of planetary nebulae (Balick 1993). Departures from spherical symmetry should then be expected also for our sources (see e.g. Silvestro et al. 1996 for a photopolarimetric study of 5 sources in our sample), and may affect even the thermal IR emission, as shown in Paper I by the elongated shape of CW Leo. Axisymmetric models of AGB circumstellar envelopes have been recently developed by Collison & Fix (1991) and Lopez et al. (1995); here basically the optical depth depends on the orientation with respect to the line of sight. These models thus introduce a new free parameter that allows one to fit the dust feature strength; we notice however that the band intensity remains unchanged with the slope of the continuum, preventing the correct fitting of LRS spectra in our “S” and “Sil+” sources. Furthermore, it is not clear why deviations from spherical symmetry should be important only for these subclasses of envelopes. We conclude that, if a correct two-dimensional treatment of the system geometry is essential for the spatial description of the IR emissions, it does not significantly affect the spectra modelling.

In IE95 the IRAS colors of sources in the $2n$ class are reproduced admitting mixtures of silicates (plus 20% crystalline olivine) and amorphous carbon (in the ratio 1:4). The possibility of such a mixing is controversial (dust formation in chemical equilibrium models predicts the depletion of the less abundant element between O and C, locked in CO molecules, see e.g. Salpeter 1974), but cannot be completely ruled out, since numerous C-rich stars display the silicate feature (see e.g. Willems & de Jong, 1986 and Le Van et al., 1992). Even though this hypothesis is unattractive, requiring the presence of mixtures only for sources of small optical depth, the others being well fitted by ordinary silicate opacities, we tested this prescription with our “S” and “Sil+” sources.

We have not obtained a real improvement in our “Sil+” model with mixed dust, because the introduction of a new fitting parameter (the silicate/carbon ratio) allowed only to reproduce the shape of the $9.8 \mu\text{m}$ feature, but not the slope of the continuum, even in the LRS region. On the other hand, in the case of the “S” source, the injection of a large quantity of amorphous carbon dust in the envelope (80% of the total) reduced the strength of the silicate feature making possible to fit the continuum in a large wavelengths range (even though the result of the fitting for the continuum is not as good as in the case of silicates only). To understand this result, one should consider that the S-stars like W And are considered objects in transition between the O-rich and the C-rich class, and thus a contamination of silicate dust in a C-rich circumstellar envelope is not at all surprising.

A third possibility to have weak silicate bands in O-rich envelopes, as required in “S” and “Sil+” LRS, without the introduction of carbonaceous dust, is to assume annealing and aging of dust grains, as proposed by Nuth & Hecht (1990). Their grain condensation scheme starts with oxydation of SiO, AlO and OH in O-rich stellar winds, producing grains character-

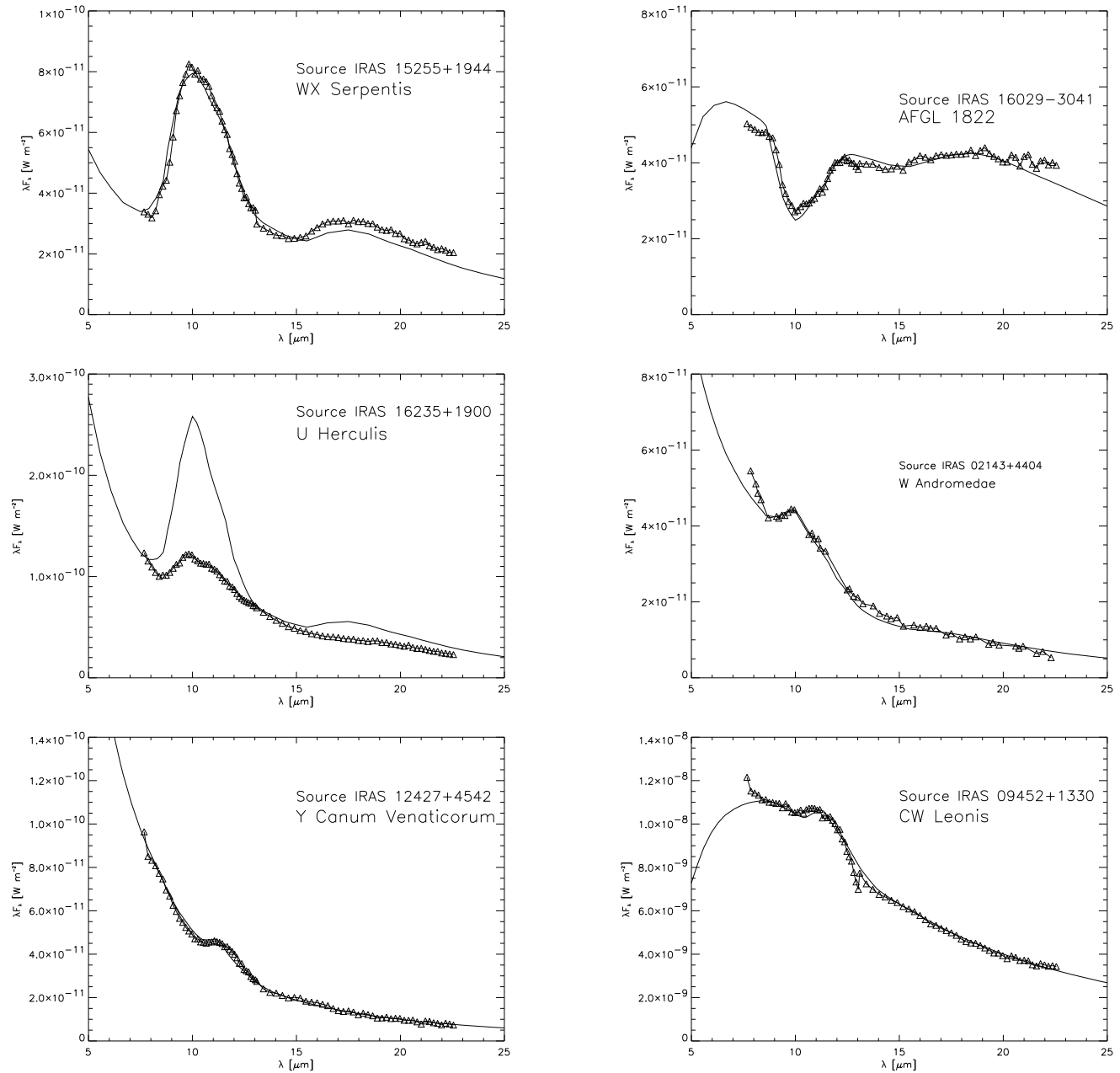


Fig. 5. Model spectra for 6 sources listed in Table 1. IRAS LRS data (triangles) are superimposed.

ized by weaker features and secondary bands at 11–13 μm ; fully grown silicates with strong features condensate only later, and are thus present only in more evolved O-rich envelopes. This view is in agreement with the classification schemes of LML90, assuming that LRS subclasses are associated with dust of different ages. If the Nuth & Hecht (1990) sequence is correct, our O-rich sources with LRS subclass other than “Sil” should be associated with envelopes with less evolved dust.

A simple semi-analytic dust shell models taking into account the presence of oxides has been developed by Onaka et al. (1989a,b). They considered a double component dust shell of silicates and aluminium oxide (Al_2O_3) with different condensa-

tion radii to fit a large sample of optically thin M Mira variables with known LRS. Choosing a larger condensation radius for the silicates, corresponding to a lower (~ 500 K) dust temperature, they were able to reproduce LRS spectra with depressed 9.8 μm feature, and thus correctly fit class “Sil+” sources. Two sources in Onaka et al. (1989b) sample are present in our list. One of them is U Her, for which they obtained a more reasonable distance determination than ours; the other is S CrB, for which the fitting results are similar. We have not tested Onaka et al. (1989a,b) prescriptions, because our model only describes single-component dust shell models. We postpone this test for a future new radiative-transfer model able to deal with multi

component shells; in fact full radiative transfer modelling is necessary even to model optically thin envelopes, as shown by IE95.

6. Conclusions

Radiative transfer modelling of circumstellar envelopes, based on simple assumptions as spherical symmetry and steady state outflows, allows detailed fitting of infrared data for single sources and the determination of system parameters as the distance, luminosity and total amount of dust ejected by the central star. The correlation with radio observations (giving informations of the total mass loss) will thus provide estimates of the dust to gas mass ratio for each modelled source. The accuracy of the fitting procedure depends mainly on the available opacities, especially in the mid-IR range where the dust features are present; a good description of the mid-IR spectra is in fact essential for the determination of the envelope optical depth and chemical composition.

The necessity of accurate spectral modelling is becoming more and more important taking into account the better spectroscopic capabilities of ground based mid-IR cameras and ISO data.

Our models confirm that the shape of carbonaceous dust features are reproduced assuming a mixture of amorphous carbon, described by AC1 Rouleau & Martin (1991) opacity, and (10%, or less) Pégourié (1988) SiC. Minor components (as PAH) might be present, but the quality of IRAS LRS do not allow their detection.

Models for O-rich envelopes associated to M and S stars suggest the possibility of different varieties of silicate dust, even if mixing between oxidic and carbonaceous dust should be considered, at least in the case of transition objects as the S-stars. If the LML90 scheme is valid, we can recognize in the Ossenkopf 1 “dirty silicates” (OS92) the correct opacity for subclass “Sil” silicates, associated to 2*n* LRS spectra and a mixture of Ossenkopf 1 “dirty silicates” (OS92) with a large amount of Rouleau & Martin (1991) AC1 amorphous carbon (in the ratio 1:4 for the subclass “S” sources). For the other subclasses accurate fits need opacities including different components of dust, other than silicates.

The dust-to-gas mass ratios we obtained are generally low (between 0.1 and 0.5 %), except in the case of the O-rich “Sil” source WX Ser (1.5%); there is a tendency for having lower dust-to-gas ratios for C-rich envelopes, but this result may be influenced by uncertainties in the average grain radius (that can be different between oxidic and carbonaceous dust) and by the inaccurate fitting of the silicate features for O-rich sources other than “Sil” subclass. New models taking into account the global dynamics of the system and coupling the dusty component with the gaseous one will allow direct correlation between IR and radio data, and will increase the accuracy in the determination of the dust-to-gas ratio, giving better insight on the dust condensation processes responsible for the mass loss in AGB stars and the formation of circumstellar envelopes.

References

- Balick, B. 1993, in: Planetary Nebulae, ed. R. Weinberger, A. Acker, Proc. IAU Symp. 155, Kluwer, Dordrecht, p. 131
- Boothroyd, A.I., Sackmann, I.J., Ahern, S.C. 1993, ApJ 416, 762
- Buss, R.H., Tielens, A.G.G.M., Snow, T.P. 1991, ApJ 372, 281
- Busso, M., Lambert, D.L., Beglio, L. 1995, ApJ 446, 775
- Busso, M., Origlia, L., Marengo, M., Persi, P., Ferrari-Toniolo, M., Silvestro, G., Corcione, L., Tapia, M., Bohigas, J. 1996, A&A 311 253
- Bussoletti, E., Colangeli, L., Borghesi, A., Orofino, V. 1987, A&AS 70, 257
- Chan, S.J., Kwok, S. 1990, A&A 237, 354
- Cherchneff, I., Barker, J.R. 1992, ApJ 416, 769
- Collison, A.J., Fix, J.D. 1991, ApJ 368, 545
- David, P., Pégourié 1995, A&A 293, 833
- Draine, B.T. 1984, ApJ 227, L71
- Draine, B.T., Lee, H.M. 1984 ApJ 285, 89
- Duley, W.W. 1993, in: Interstellar Dust, ed. L.J. Allamandola, A.G.G.M. Tielens, Proc. IAU Symp. 135, Kluwer, Dordrecht, p.141
- Frost, C.A., Lattanzio, J.C. 1996, in proc. “Stellar Evolution: What Should Be Done”; 32nd Liège Int. Astroph. Coll., 1995, in press
- Griffin, I.P. 1990, MNRAS 247, 591
- Griffin, I.P. 1993, MNRAS 260, 831
- Groenewegen, M.A.T. 1993, Ph.D. thesis, Univ. of Amsterdam
- Habing, H.J. 1996, A&AR 7, 97
- Hashimoto, O. 1995, ApJ 442, 286
- Harvey, P.M., Lester, D.F., Brock, D., Joy, M. 1991 ApJ 368, 558
- IRAS Catalogues and Atlases, Atlas of Low Resolution Spectra 1986, Iras Science Team. A&AS 65, 607
- Ivezić, Ž., Elitzur, M. 1995, ApJ 445, 415 (IE95)
- Ivezić, Ž., Elitzur, M. 1996a,b, MNRAS in, press
- Jones, A.P., Duley, W.W., Williams, D.A. 1990, QJRAS 31, 567
- Jones, T.W., Merrill, K.M. 1976, ApJ 389, 400
- Jura, M. 1996, ApJ in, press
- Justanont, K., Tielens, A.G.G.M. 1992, ApJ 389, 400
- Käufel, H.U., Jouan, R., Lagage, P.O., Mase, P., Mestreau, P., Tarrus, A. 1992, The Messenger 70, 67
- Krätschmer, W., Huffmann, D.R. 1978, Ap&SS 61, 195
- Krüger, D., Gauger, A., Sedlmayr, E. 1994, A&A 290, 573
- Little-Marenin, I.R., Little, S.J. 1990, AJ 99, 1173 (LML90)
- Le Van, P.D., Sloan, G.C., Little-Marenin, I.R., Grasdalen, G.L. 1992 ApJ 392, 702
- Lopez, B., Mékarnia, D., Lefèvre, J. 1995 A&A 296, 752
- Loup, C., Forveille, T., Omont, A., Paul, J.F. 1993, A&AS 99, 291
- Martin, P.G., Rogers, C. 1987, ApJ 322, 374
- Mathis, J.S., Rumpl, W., Nordsieck, K.H. 1977, ApJ 217, 425
- Nuth, J.A.III, Hecht, J.H. 1990, Ap&SS 163, 79
- Omont, A., Loup, C., Forveille, T., te Lintel Hekkert, P. Habing, H., Sivagnanam, P. 1993, A&A 267, 515
- Onaka, T., de Jong, T., Willems, F.J. 1989a, A&A 218, 169
- Onaka, T., de Jong, T., Willems, F.J. 1989b, A&AS 81, 261
- Ossenkopf, V., Henning, Th., Mathis, J.S. 1992 A&A 261, 567 (OS92)
- Pégourié, B. 1988, A&A 194, 335
- Pégourié, B., Papoular, R. 1985, A&A 142, 451
- Puget, J.L., Léger, A. 1989, ARA&A 27, 261
- Rouleau, F., Martin, P.G. 1991, ApJ 377, 526
- Rowan-Robinson, M. 1980, ApJS 44, 403
- Salpeter, E.E. 1974, ApJ 193, 579

- Silvestro, G., Roseo, E., Marengo, M., Busso, B., Origlia, L., Scaltriti, F. 1996, in proc. I Torino Workshop: Evolution and Nucleosynthesis in AGB Stars and Their Descendants, ed. M. Busso and R. Gallino
- Schönberner, D., Steffen, M., Stahlberg, J., Kifonidis, K., Blöker, T. 1996, in proc. IAU Symposium 177, “The Carbon Star Phenomena”, Antalya, Turkey, May 27-31, 1996
- Simpson, J.P. 1991, ApJ 368, 570
- Skinner, C.J., Whitmore, B. 1988, MNRAS 237, 79
- Sopka, R.J., Hildebrand, R., Jaffe, D., Gatley, I., Roelling, T. 1985, ApJ 294, 242
- Stencel, R.E., Nuth, J.A.III, Little-Marenin, I.R., Little, S.J. 1990 ApJ 350, L45
- Straniero, O., Gallino, R., Busso, M. et al. 1995, ApJ 440, L85
- van der Veen, W.E.C.J, Habing, H.J. 1988, A&A 194, 125
- Vassiliadis, C., Wood, P.R. 1993, ApJ 413, 641
- Volk, K., Kwok, S. 1988, ApJ 331, 435
- Willems, F.J., de Jong, T. 1986, ApJ 309, L39
- Wood, P.R., Bessel, M.S., Fox, M.W. 1983, ApJ 272, 99

This article was processed by the author using Springer-Verlag \TeX A&A macro package version 4.